Petroleum Science 23 (2026) 2560–2573

Contents lists available at ScienceDirect

Petroleum Science

journal homepage: www.keaipublishing.com/en/journals/petroleum-science

Original Paper

Research and application of thin sandstone identification technique based on post-stack seismic data: A case study of Ecuador's M reservoir

Qi-Ming Zheng [a], Hui Chen [b,*], Qiu-Xiang Zhu [b], Xue-Xiang Gu [a], Hai Xu [c,d], Fa-You Li [c], Ben-He Cheng [d], Yu-Liang Feng [d], Chuan Wang [d]

[a] School of Earth Sciences and Resources, China University of Geosciences (Beijing), Beijing, 100083, China
[b] Geomathematics Key Laboratory of Sichuan Province, Chengdu University of Technology, Chengdu, 610059, Sichuan, China
[c] Research Institute of Petroleum Exploration and Development, Sinopec (Beijing), Beijing, 102206, China
[d] Sinopec International Petroleum Exploration and Production Corporation (Beijing), Beijing, 100029, China

ARTICLE INFO

Article history:
Received 21 April 2025
Received in revised form
9 November 2025
Accepted 13 January 2026
Available online 18 January 2026

Edited by Meng-Jiao Zhou

Keywords:
Reflection coefficient
Time-variant wavelet
Denoising
Signal-to-noise ratio
Thin reservoir prediction

ABSTRACT

The M sandstone member within the Cretaceous Napo Formation is a critical hydrocarbon reservoir in the Oriente Basin's foredeep belt. However, its characterization is severely challenged by its thin-bed nature (2–8 m) and rapid lateral facies variations. The available 3D seismic data has a dominant frequency of about 45 Hz, yielding an apparent resolution of approximately 26 m. Conventional seismic techniques, such as deconvolution, spectral whitening, and inverse Q filtering, rely on stationary wavelet assumptions and are sensitive to noise and parameter inaccuracies. This limitation leads to the misinterpretation of the "isolated reservoir" in the M01 well, which has long hindered progress in exploration and development in the area. To address these challenges, we develop a novel high-resolution seismic processing workflow centered on precise reflectivity inversion. Our approach systematically integrates three key innovations: First, targeted denoising is applied to enhance the signal-to-noise ratio, ensuring the stability of subsequent inversion. Second, we overcome the stationary wavelet assumption of conventional methods by employing the generalized S-transform to construct a discrete, time-varying wavelet library, which accurately captures the seismic wavelet's frequency attenuation with depth. Third, we integrate this time-varying wavelet model with a reflectivity inversion algorithm based on odd-even reflection theory and a least-squares optimization, enabling high-fidelity recovery of thin-layer reflection coefficients. The application of this workflow in the M Oilfield yields a transformative improvement in seismic resolution. The processed data achieves a significant broadening of the effective frequency bandwidth, elevating the dominant frequency from 45 Hz to 85 Hz. This enhancement consequently improves the theoretically detectable thickness from approximately 14 m to approximately 5 m. Most importantly, the processed seismic profiles clearly delineate ultra-thin sand bodies, ranging from 3 to 5 m, with drilling results exhibiting high consistency with seismic interpretation (e.g., successful wells M01 and M05-2 versus dry wells M05 and M05-1). The resulting seismic attributes also reveal clearer geological features, such as delta outlines and underwater distributary channels. This study successfully resolves the exploration dilemma that persisted in the area for over two decades, overturning the "isolated reservoir" model and revealing the continuous distribution characteristics of the M sandstone. The demonstrated workflow provides a robust and systematic solution for characterizing thin-bed reservoirs, directly leading to increased exploration success. The established technical framework offers a valuable and practical reference for the detailed exploration and development of similar thin sandstone reservoirs in foredeep and slope settings worldwide.

* Corresponding author.
E-mail address: huichencdut@cdut.edu.cn (H. Chen).

Peer review under the responsibility of China University of Petroleum (Beijing).

https://doi.org/10.1016/j.petsci.2026.01.013

1. Introduction

High-resolution seismic data processing has emerged as a critical discipline in petroleum geophysics, driven by the increasing demand for accurate characterization of thin-bed reservoirs in complex depositional systems (Yilmaz, 1987; Widess, 1973). Conventional high-resolution techniques, including deconvolution (Yun et al., 2022; Wang et al., 2003), time-varying spectral whitening (Zhao et al., 2021; Jiang et al., 2018), and inverse Q filtering (Zhao et al., 2021; Li et al., 2021), have been widely applied to enhance seismic resolution. These methods aim to compress wavelet signatures, flatten amplitude spectra, or compensate for attenuation effects. However, their effectiveness is constrained by fundamental assumptions and practical limitations.

Deconvolution algorithms, such as spiking deconvolution and predictive deconvolution, rely on stationary wavelet models and sparse reflection coefficient assumptions (Yun et al., 2022). This approach often fails in geologically complex settings where wavelet characteristics vary with depth and lateral position. Moreover, deconvolution's sensitivity to high-frequency noise introduces artifacts that degrade signal quality, particularly in data with low signal-to-noise ratios (SNR) (Yilmaz, 1987).

Spectral whitening techniques attempt to enhance resolution by equalizing amplitude spectra across frequencies (Du et al., 2019). However, this method assumes stationary wavelet properties and ignores the time-varying nature of seismic wavelets caused by lithological changes and attenuation effects (Wang et al., 2015). As a result, whitened seismic traces often exhibit phase distortion and reduced continuity of weak reflections.

Inverse Q filtering addresses attenuation compensation by estimating absorption parameters from seismic data (Zhao et al., 2021). The accuracy of this method depends critically on reliable Q-factor models, which are challenging to derive in areas with lateral variations in lithology and fluid saturation (Li et al., 2021). Errors in Q-factor estimation can lead to overcompensation or undercompensation, degrading resolution improvements.

A significant breakthrough occurred in 2005 with the introduction of post-stack spectral inversion by Castagna et al. (2003). This method decomposes seismic data into frequency bands, inverting each band to derive reflection coefficients that preserve thin-bed information below tuning thickness (Castagna, 2003; Chopra et al., 2006). By focusing on spectral components sensitive to thin layers, spectral inversion has demonstrated improved reservoir characterization capabilities.

Despite above methods have achieved certain application effects, current methodologies remain limited by two key issues. First, most approaches employ fixed deterministic or statistical wavelets, which cannot adapt to the time-varying wavelet characteristics inherent in real seismic data (Zhu et al., 2022; Wang et al., 2025). Second, noise suppression strategies often overlook the impact of random noise on small reflection coefficients, particularly in low SNR environments (Jiang et al., 2018). These limitations compromise the accuracy of reflection coefficient inversion and thin-bed identification, necessitating the development of adaptive, noise-robust processing workflows.

2. Geological setting

The Oriente Basin, located within Ecuador, is a critical component of the Andean foreland basin system. Its tectonic evolution and sedimentary filling processes completely record the coupled response to the subduction of the Pacific Plate and the Andean orogeny from the Mesozoic to the Cenozoic (as shown in the red box in Fig. 1). In terms of tectonic evolution stages, during the Cretaceous period, under the control of regional extensional tectonics, the basin was in a passive continental margin setting, developing marine sedimentary sequences (Baby et al., 2013). Entering the Cenozoic era, concomitant with the uplift of the Andes, the basin transformed into a foreland basin, with its depositional systems gradually transitioning to continental fluvial-deltaic systems. It is noteworthy that the most promising reservoirs for oil and gas exploration within the basin are concentrated in the Cretaceous marine sequences. Among these, the thin tidal sandstones developed in the Napo Formation during the mid-late Cretaceous (Albian-Cenomanian) are the current key target zones for oil and gas exploration (Fu et al., 2019).

The study area is located on the structural slope with reverse faults in the foredeep zone of the Oriente Basin (Fig. 2(a)), where structural-lithologic composite hydrocarbon reservoirs are developed, and the M sandstone member is the sole target horizon for rolling exploration and development in this region. The 3D seismic exploration coverage area of the study area is approximately 500 km^2, which is formed by splicing multiple blocks of 3D seismic data acquired before 2006, with a fold coverage of 30–60 times and a dominant seismic frequency of about 45 Hz. The apparent resolution calculated based on the quarter-wavelength is approximately 26 m. The M reservoir has a burial depth of about 3048 m (approximately 10,000 feet) and belongs to the tidal flat facies sandstone deposits of the Cretaceous Napo Formation, with drastic lateral facies changes; the sandstone thickness ranges from 2 m to 8 m, the porosity is usually 15%–25%, and the permeability is generally in the range of 1000–10000 mD (Zhu et al., 2024). From the drilling practice (Fig. 2(b)), it is known that among the three wells (M01, M02, M03) drilled in 1994, Wells M02 and M03 did not encounter effective hydrocarbon reservoirs (being dry wells), and only Well M01 encountered the M sandstone with a thickness of 2.83 m. This well maintained a stable production state for a long time, with a daily oil production of about 500 bbl/d, and the cumulative oil production reached 68×10^4 t by 2018; however, Well MP01 drilled in 2011 and Well M05 drilled in 2018 also did not encounter effective hydrocarbon reservoirs. Due to the inability of the resolution of conventional seismic data to accurately characterize the spatial distribution characteristics of the M sandstone member, Well M01 was mistakenly determined as an “isolated oil reservoir”, which in turn led to long-term stagnation in the rolling exploration and development work in this region.

In addition, the exploration of the M thin-bedded tidal sandstones also faces many technical and geological bottlenecks: the migration of tidal channels and the development of interbedded mudstones lead to rapid lateral facies changes of the reservoir, and the connectivity shows strong heterogeneity (Li et al., 2024); the resolution of conventional seismic exploration technology cannot effectively distinguish the acoustic impedance difference between sandstones and mudstones, resulting in ambiguous characterization of sandbody boundaries; calcite cementation and clay mineral filling during the diagenetic process not only reduce the reservoir porosity but also form seepage barriers; the development of the paleotidal system is controlled by multiple factors such as shelf slope, tidal range, and high-frequency sea-level fluctuations, and the spatial configuration relationship of tidal flat-tidal channel microfacies is complex, which increases the difficulty of sedimentary facies modeling. The superposition of these factors collectively restricts the prediction accuracy of subtle hydrocarbon accumulation in thin-bedded sandstones (Ameneiro et al., 2020).

3. Theoretical basis and influencing factors

In 2004, Tirado established a simplified two-point reflection coefficient model, demonstrating that amplitude and frequency

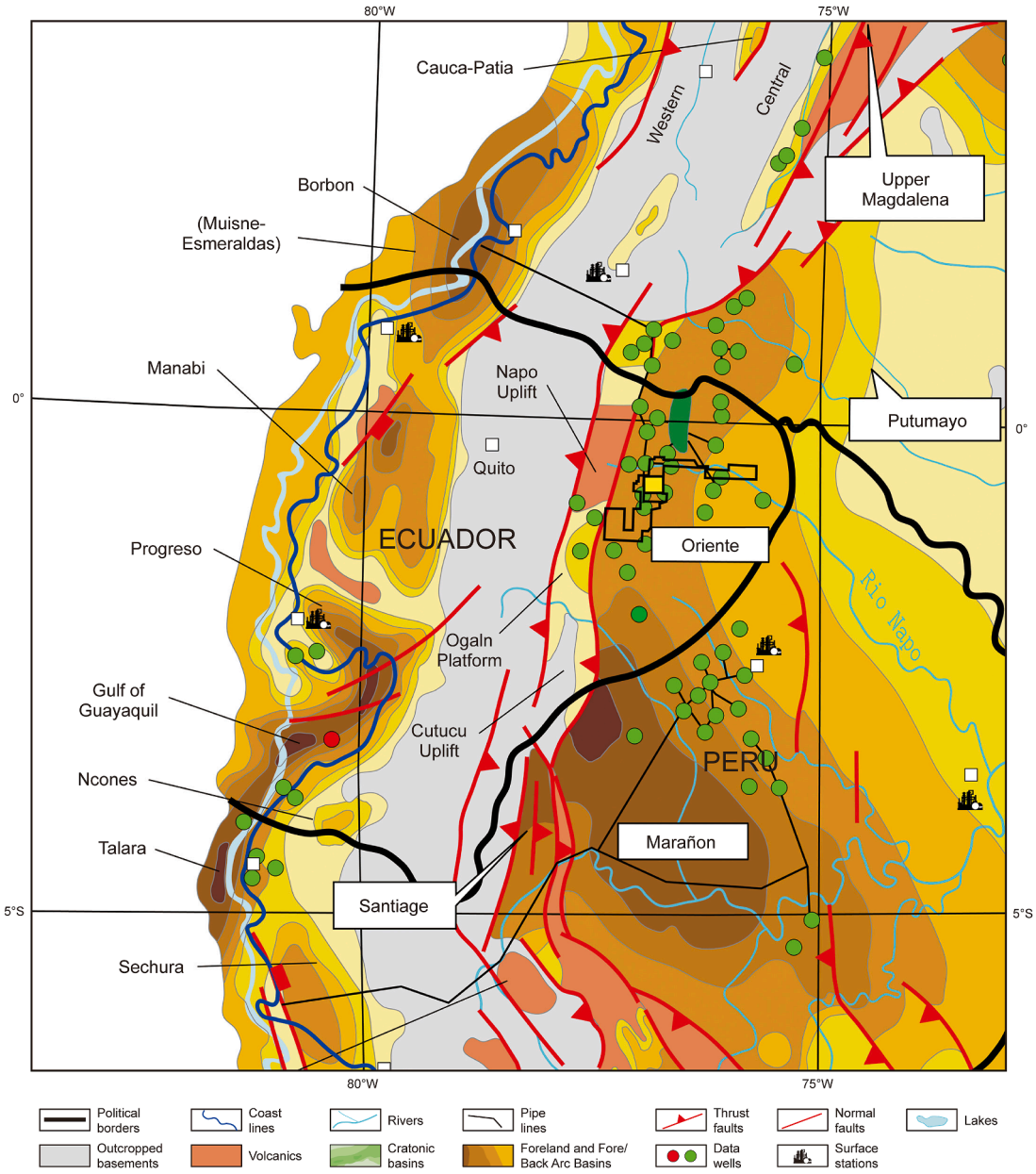

Fig. 1. Regional geological map of the Oriente Basin.

continue to change even when the layer thickness is below the tuning thickness. By utilizing the parity decomposition of the reflection coefficient, frequencies outside the effective band can be recovered, enabling the prediction of formation thicknesses below the seismic sampling rate. Spectral inversion theory treats the reflection coefficients in seismic records as a series of pulse signals. Let $R(t_i)$ denote the reflection coefficient of the effective seismic signal at time t_i in a given seismic reflection trace. Then,

$$R(t_i) = \alpha_i + \beta_i \tag{1}$$

where α_i and β_i represent the odd and even reflection coefficients of the effective seismic signal at time position t_i, respectively (Fig. 3). According to the Fourier transform, the reflection coefficient spectrum of the effective seismic signal is:

$$R(f) = \alpha_i e^{(-i2\pi t_i f)} + \beta_i e^{(-i2\pi t_i f)} \tag{2}$$

In practice, solving the reflection coefficient involves decomposing the seismic signal using a wavelet library, which requires high-SNR seismic data. The convergence of the objective function is influenced by the inversion wavelet and noise. Therefore, the intensity of noise and the degree of matching between the inversion wavelet and the actual seismic wavelet affect the accuracy of the reflection coefficient solution.

Fig. 4(a) shows the thin reservoir reflection coefficient model, Fig. 4(b) displays the 30 Hz Ricker wavelet, and Fig. 4(c) presents the synthetic trace generated by convolving the 30 Hz forward wavelet with the reflection coefficient. To understand the impact of noise on inversion results, 15% random noise was added to the synthetic record (Fig. 4(d)).

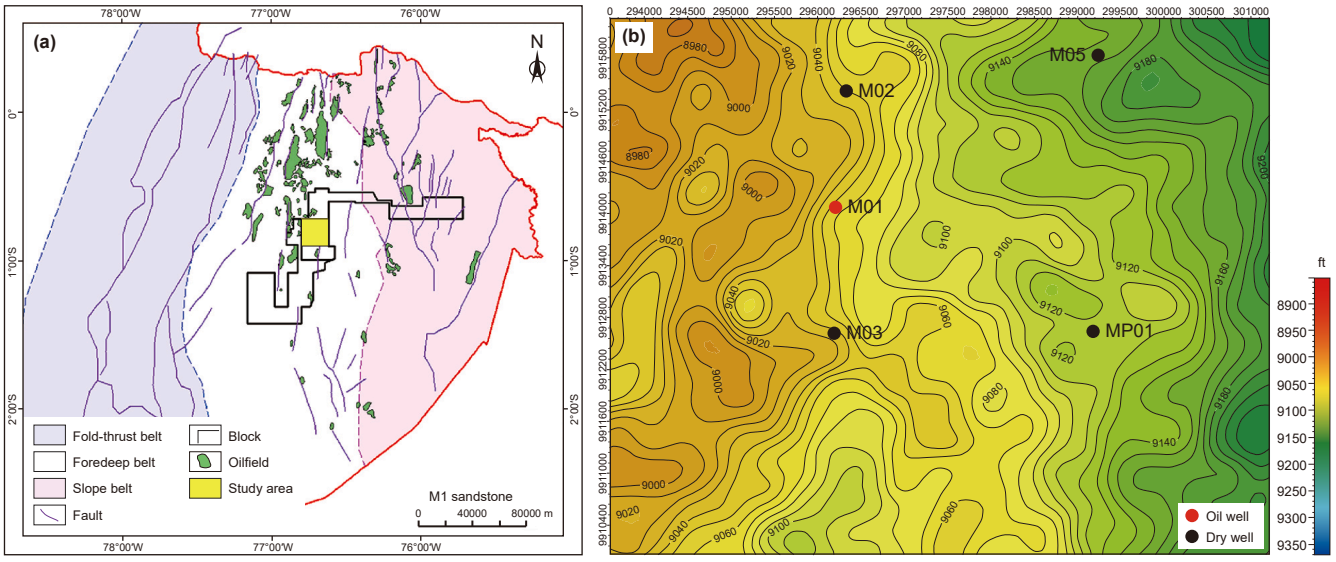

Fig. 2. Map of drilling distribution and tectonic location of M oil reservoir.

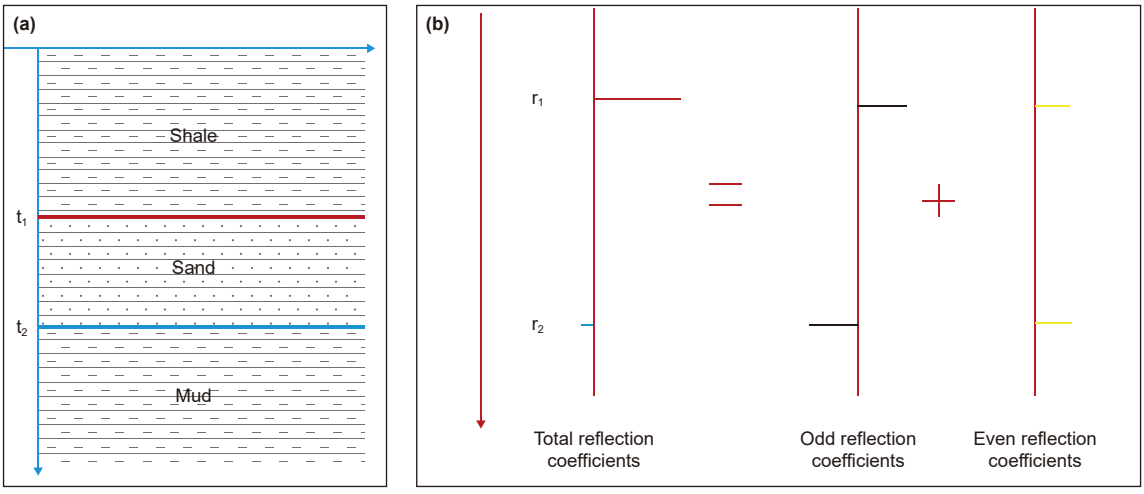

Fig. 3. Theoretical model of odd-even reflection.

When the reflection coefficient is calculated using an incorrect wavelet, the results obtained with 25 Hz and 35 Hz wavelets (Fig. 5(a) and (c)) are inferior to those obtained with the correct 30 Hz wavelet (Fig. 5(b)). Furthermore, the results of reflection coefficient inversion with and without noise differ significantly (Fig. 5(b) and (d)).

4. Research methods

To further enhance the accuracy of reflection coefficient estimation and signal recovery, this study adopts a systematic high-resolution processing workflow, the core steps of which are illustrated in Fig. 6. The procedure begins with frequency-division denoising to improve the signal-to-noise ratio. Subsequently, a discrete wavelet library is constructed based on the generalized S-transform, establishing a dynamic time-frequency-varying wavelet function to better adapt to the time-varying characteristics of wavelets. This time-varying function is then integrated with spectral inversion technology to derive a more accurate reflection coefficient series. Finally, signal reconstruction is performed via wavelet transform, yielding a high-resolution seismic data volume.

4.1. Denoising and effective signal scanning

Seismic data often contain noise due to acquisition and processing methods. Directly expanding the effective bandwidth of seismic signals can reduce the SNR and the reliability of reservoir reflection signals. To improve the stability of the reflection coefficient, denoising methods for coherent and random noise are applied to enhance the SNR (Ma et al., 2016; Ou Yang et al., 2019; Wang et al., 2019). This study employs principal component analysis (PCA) for noise removal. The PCA is implemented using its default configuration, which retains principal components based on the cumulative variance contribution ratio, a statistically robust criterion for signal-noise separation (Tong et al., 2023). An iterative process is applied, wherein the initially separated noise component is reprocessed to recover residual effective signals, which are then incorporated back into the primary data. Fig. 7(a)–(d) show the original low-pass and band-pass filtered data and the

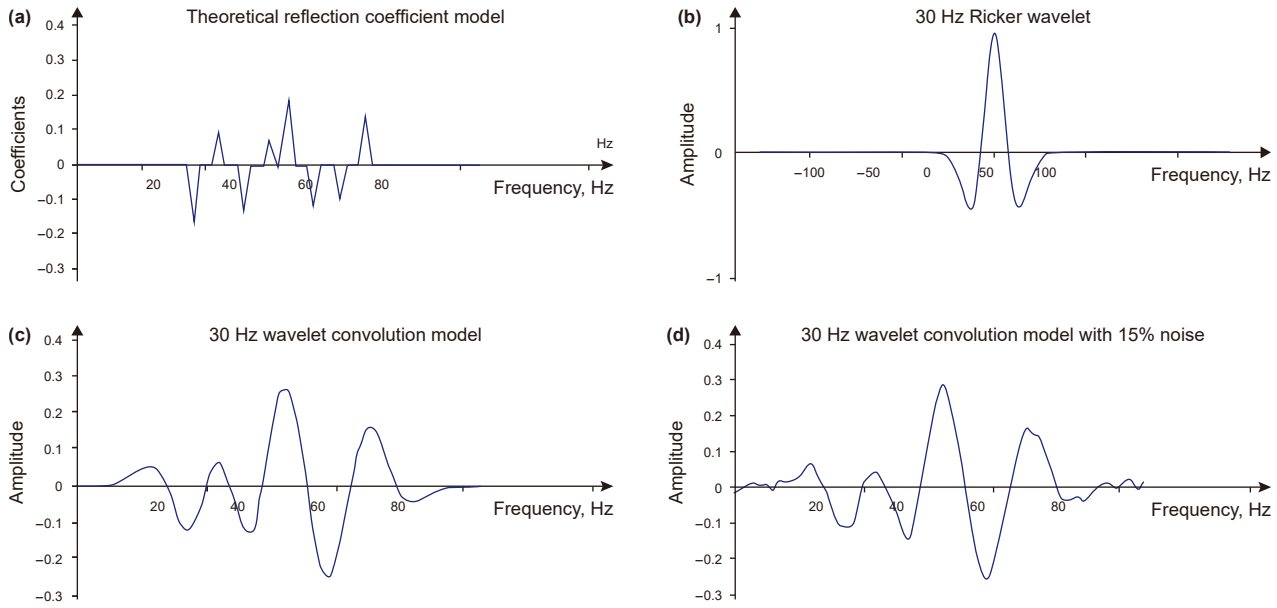

Fig. 4. Influence of wavelet and noise on reflection coefficient.

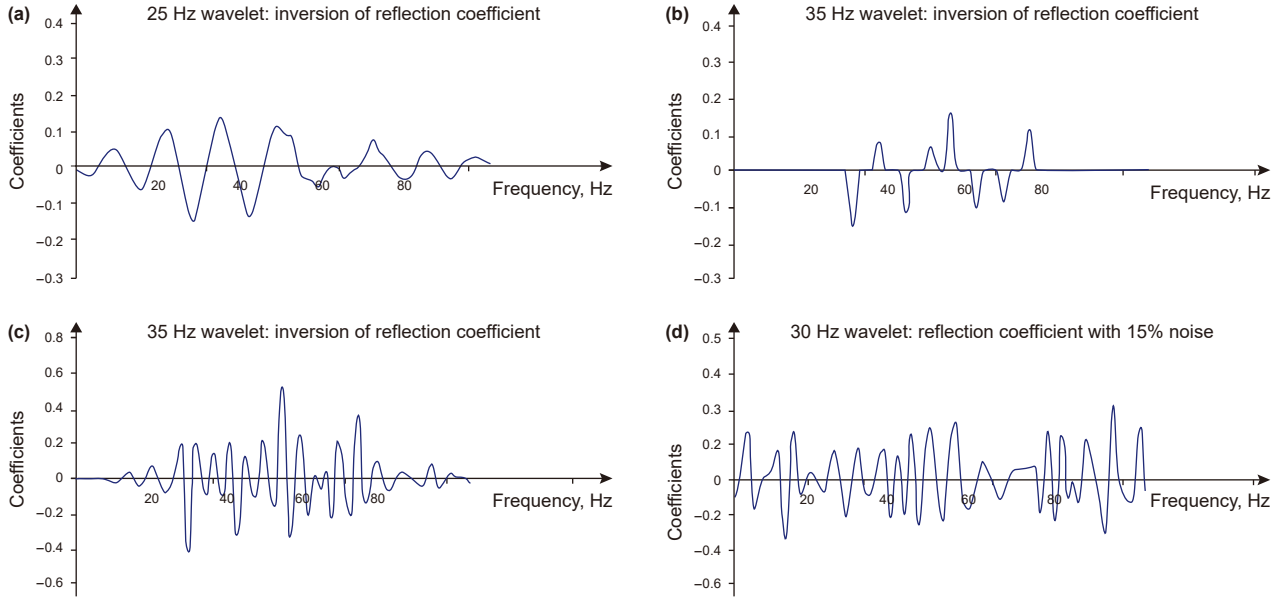

Fig. 5. Influence of wavelet and noise on reflection coefficient.

separated noise data, while Fig. 7(e) and (f) display the high-pass filtered data before and after denoising. The results indicate that effective seismic signals above 115 Hz are preserved.

4.2. Wavelet library and time-varying wavelet function

Characterizing non-stationary seismic signals requires advanced time-frequency analysis techniques. Early methods like Short-Time Fourier Transform (STFT) and Continuous Wavelet Transform (CWT) provided foundational tools (Gabor, 1946; Morlet et al., 1982), but their fixed resolution or redundancy limited applications. The Hilbert-Huang Transform (HHT) later addressed non-stationarity through empirical mode decomposition (Huang et al., 1998), though reproducibility challenges persisted.

Stockwell et al. (1996) introduced the S-transform, combining STFT localization with CWT scalability using adaptive Gaussian windows. This innovation enabled time-frequency analysis with improved resolution trade-offs. However, its fixed window shape constrained adaptability in complex geological scenarios.

To address this limitation, Chen et al. (2008) developed the Generalized S-Transform (GST), introducing parameters rgs and ρ to dynamically adjust window shape and frequency focusing. This enhancement allows GST to adapt to varying signal characteristics, particularly critical for seismic data with time-varying wavelet properties (Pinnegar et al., 2003; Gao et al., 2003). The mathematical formulation of GST is:

$$\mathrm{GST}(x(\tau,f)) = \int_{-\infty}^{+\infty} \frac{|f|^{\mathrm{rgs}}}{\sqrt{2\pi}\rho} \exp\left[-\frac{(\tau-t)^2 f^{2\mathrm{rgs}}}{2\rho^2}\right] \exp(-i2\pi f t)\mathrm{d}t \quad (3)$$

where τ is the translation parameter, f is frequency. The parameters rgs and ρ both have the function of changing the width and

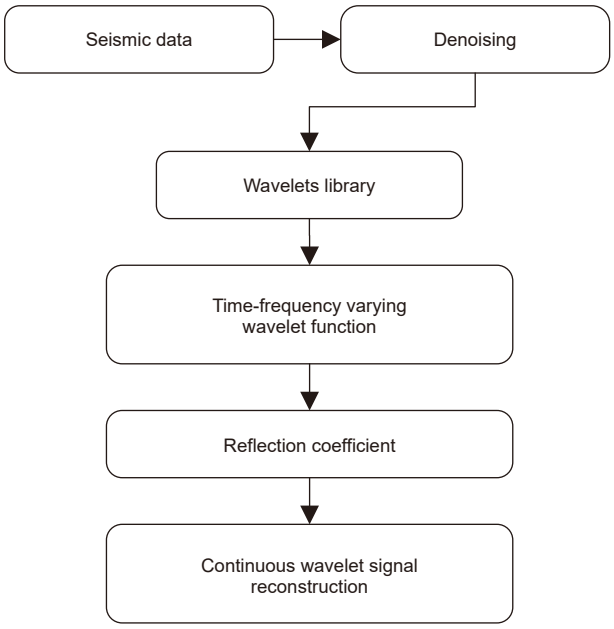

Fig. 6. Seismic signal reconstruction process based on variable time-frequency wavelet.

amplitude of the time window function. According to the needs of actual application, rgs and ρ can be reasonably selected to adjust the time-frequency resolution of the generalized transformation, overcoming the problem that the change trend of the time window function in the transformation is fixed, making the generalized transformation more practical and flexible.

Due to the varying positions of seismic traces (Fig. 8), the extracted wavelets exhibit unstable side lobes and frequency changes, leading to poor wavelet consistency and unstable reflection coefficient solutions (Zhang et al., 2021). To address wavelet inconsistency, a time-varying frequency wavelet attenuation function is established based on the recorded wavelets in the library:

$$r(t) = \left[1 - 2(\pi f_0 t)^2\right]\exp\left[-(\pi f_0 t)^2\right] \tag{4}$$

where f_0 represents the dominant frequency of the seismic wavelet, and $r(t)$ is the Ricker wavelet function.

Table 1 shows the dominate frequency, high and low frequency cutoff frequencies of wavelets obtained from the energy envelope (Fig. 9).

The time-varying dominant frequency characteristics of seismic wavelets were analyzed using single-trace energy spectrum analysis (Fig. 9). To model the observed frequency attenuation with depth, a logarithmic decay function was fitted to the dominant frequency variation data (Fig. 10). The fitting process employed least-squares regression to minimize discrepancies between measured frequencies and the logarithmic model. The logarithmic decay function is fitted:

$$f_0 = 201.1 - 21\ln(t) \tag{5}$$

Fig. 10 demonstrates the high-quality fit between the logarithmic function and empirical data. This result validates the assumption of systematic frequency attenuation with increasing travel time, likely due to seismic wave absorption and dispersion effects. The derived coefficients (201.1 and −21) capture the initial dominant frequency and decay rate, respectively. Substituting Eq. (5) into Eq. (4) yields the time-varying frequency wavelet function:

$$W(t) = \left[1 - 2(\pi_0 t\cdot(201.1 - 21\ln(t)))^2\right]\cdot\exp\Big[- (\pi_0 t(201.1 - 21\ln(t))t)^2\Big] \tag{6}$$

4.3. Reflection coefficient and signal reconstruction

According to the principle of seismic signal processing, the seismic signal in frequency domain can be expressed as (Puryear and Castagna, 2008; Zhu et al., 2022):

$$S(f) = W(f)R(f) + N(f) \tag{7}$$

where $S(f)$ is seismic record, $W(f)$ is the time-frequency variable seismic wavelet, $R(f)$ is the reflection coefficient, $N(f)$ is the noise, and f represents the frequency.

$$S(f) = W(f)\left[\alpha_i e^{(-i2\pi t_i f)} + \beta_i e^{(-i2\pi t_i f)}\right] + N(f) \tag{8}$$

where α_i and β_i are the odd and even reflection coefficients, respectively, and t_i is the time corresponding to the reflection coefficients (Chen et al., 2015). The reflection coefficient spectrum can be expressed as:

$$\frac{S(f)}{W(f)} = \alpha_i e^{(-i2\pi t_i f)} + \beta_i e^{(-i2\pi t_i f)} + \frac{N(f)}{W(f)} \tag{9}$$

The items are

$$\frac{N(f)}{W(f)} = \frac{S(f)}{W(f)} - \alpha_i e^{(-i2\pi t_i f)} - \beta_i e^{(-i2\pi t_i f)} \tag{10}$$

For any frequency $f_m, (m = 1,2,\cdots,M)$, then Eq. (10) is expressed as:

$$\frac{N(f_m)}{W(f_m)} = \frac{S(f_m)}{W(f_m)} - \alpha_m e^{(-i2\pi t_m f_m)} - \beta_m e^{(-i2\pi t_m f_m)} \tag{11}$$

We define the objective function as $F(\alpha,\beta)$:

$$F(\alpha_m,\beta_m) = \sum_{i=1}^{k}\left(\sum_{j=1}^{N}\left(\sum_{m=1}^{M}\left(\frac{S(f_m)}{W(f_m)} - \alpha_m e^{(-i2\pi t_m f_m)} - \beta_m e^{(-i2\pi t_m f_m)}\right)\right)\right)^2 \tag{12}$$

where K represents the sampling point in the time window, and N represents the number of seismic channels. Here, $F(\alpha,\beta)$ uses the least squares method to achieve the minimum value, and solves α_i and β_i.The reflection coefficient obtained by the least square method is shown in Fig. 11.

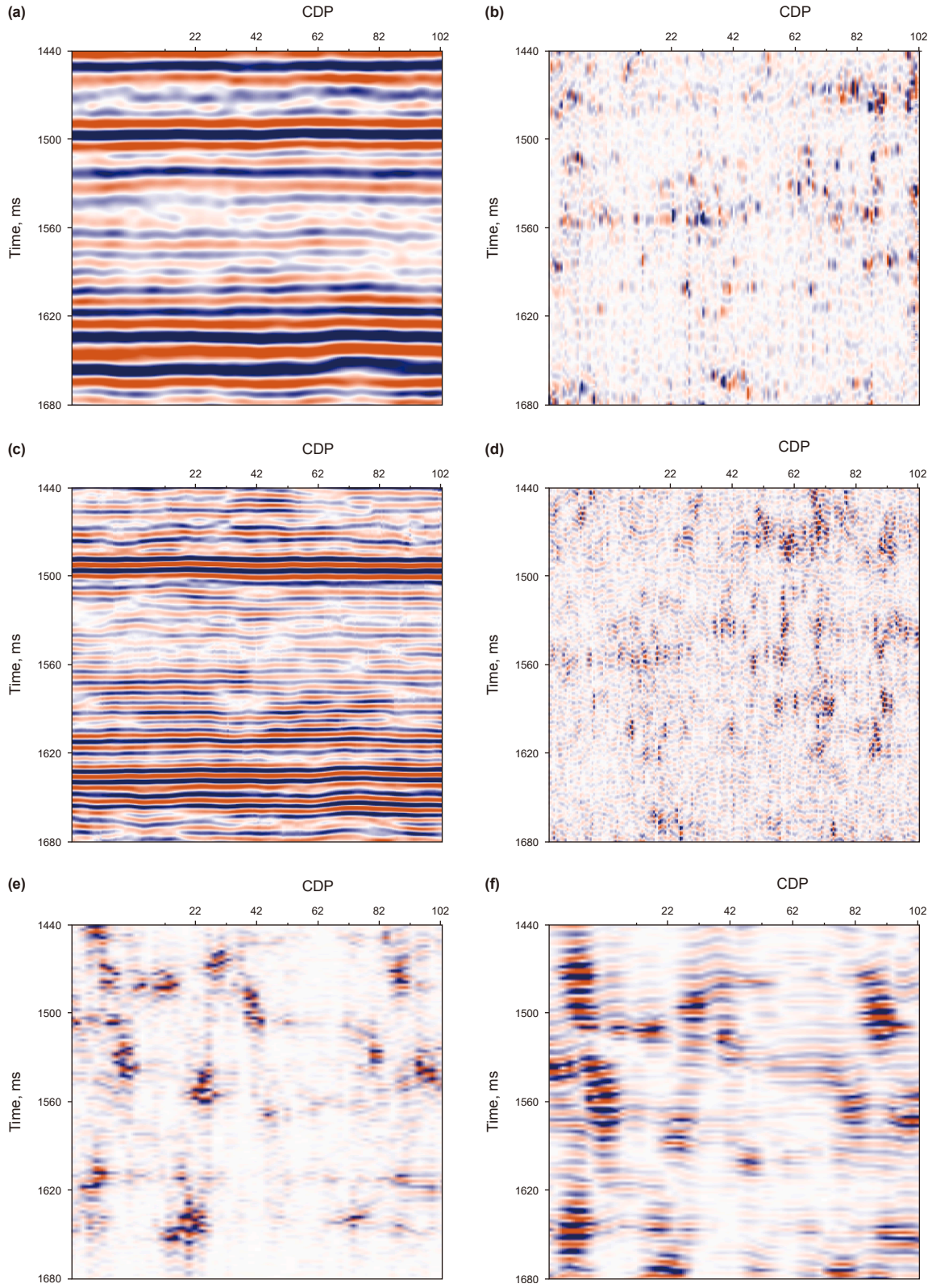

Fig. 7. Frequency division denoising and effective signal scanning: **(a)** low-pass data below 25 Hz, **(b)** low-pass noise, **(c)** band-pass data between 25 Hz and 85 Hz, **(d)** band-pass noise, **(e)** high-pass data above 115 Hz, **(f)** high-pass denoising data.

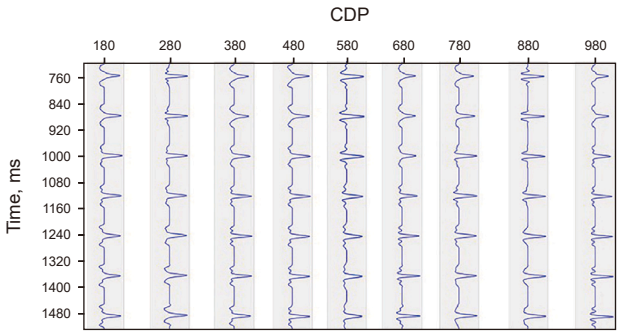

Fig. 8. Wavelets in different seismic tracks.

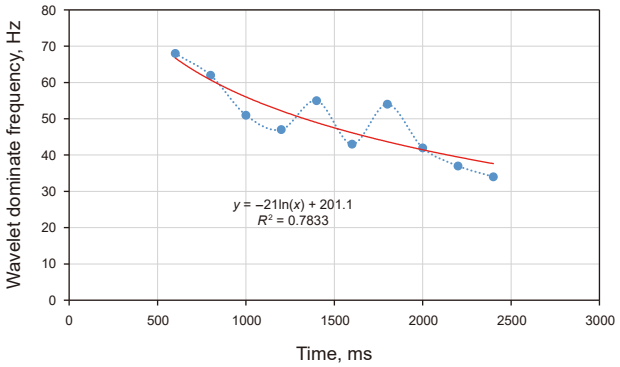

Fig. 10. Fitting diagram of logarithmic function of time-varying main frequency.

Table 1
Dominate frequency, high and low cut frequency values of wavelets at different times.

Time, ms	f_0, Hz	Low f, Hz	High f, Hz
600	68	8	89
800	62	8	83
1000	51	8	78
1200	47	8	80
1400	55	8	78
1600	43	8	78
1800	54	8	70
2000	42	8	67
2200	37	8	65
2400	34	8	56

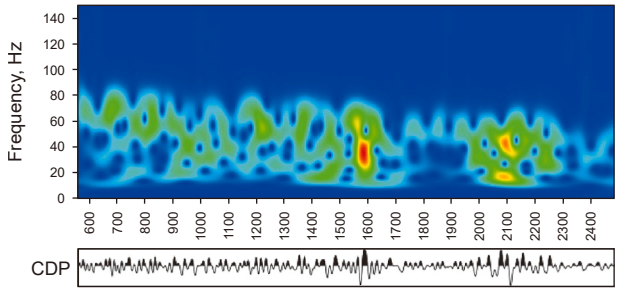

Fig. 9. Diagram of single-trace energy spectrum of dominant frequency, high and low cut frequency.

Let the reflection coefficient be $f(t) \in L^2(R)$, the wavelet generating function is $\Psi(t)$, then the inverse transform condition of the continuous wavelet transform is:

$$C_\Psi = \int_R \frac{|\Psi(\omega)|^2}{\omega} \mathrm{d}\omega < \infty \tag{13}$$

where $\Psi(\omega)$ is the Fourier transform of $\Psi(t)$, and C_Ψ is the corresponding wavelet constant. Then, the formula of continuous wavelet transform in the time domain is expressed as (Smith et al., 2008):

$$C_\Psi(a,\tau) = [f(t), \Psi_{a,\tau}(t)] = \int_{-\infty}^{+\infty} f(t) \frac{1}{\sqrt{a}} \overline{\Psi}\left(\frac{t-\tau}{a}\right) \mathrm{d}t \tag{14}$$

where $C_\Psi(a,\tau)$ is the time frequency spectrum, a is the scale parameter with the wavelet center frequency as the reference, and τ is the translation parameter. The comparison between the original spectrum and the transformed spectrum is shown in Fig. 12.

4.4. Verification with synthetic seismic data

To verify the effectiveness of the high-resolution processing technique proposed in this study for identifying thin sandstone reservoirs in the M formation, the M01 well, which has been confirmed to contain oil in the study area, was selected as the verification well. Based on logging data such as density and acoustic impedance from this well, synthetic seismic records with different dominant frequencies were generated through convolutional forward modeling. Ricker wavelets with dominant frequencies of 45 Hz, an intermediate frequency of 65 Hz, and 85 Hz were selected to simulate the seismic response characteristics of the M reservoir at different resolution levels, thereby establishing a correlation between enhanced resolution and log interpretation.

The synthetic record results (Fig. 13) show that in the 45 Hz dominant frequency synthetic record, the M reservoir is affected by the tuning effect, with overlapping reflections from sandstone and mudstone appearing blurred, making it impossible to distinguish the top and bottom boundaries of the reservoir. In the 65 Hz dominant frequency synthetic record, weak reflections from the reservoir can be observed, but the reflection signals still partially overlap, allowing only for the identification of the reservoir's presence. In the 85 Hz dominant frequency synthetic record, the M reservoir exhibits a complete and clear trough response characteristic, with reflections from the sandstone-mudstone interfaces fully separated, and the seismic events of the reservoir's top and bottom boundaries clearly visible.

This verification result demonstrates that the technique proposed in this study, which elevates the dominant frequency to 85 Hz, is scientifically sound and effectively meets the requirements for detailed identification of thin sandstone reservoirs in the M formation. It provides reliable technical validation for subsequent “real data” processing and application.

5. Field application

The Andes Project is situated in the Oriente Basin of Ecuador, South America, adjacent to the Putumayo Basin in Colombia and the Marañón Basin in Peru. Covering an area of approximately 100,000 square kilometers, the Oriente Basin is an oil-bearing

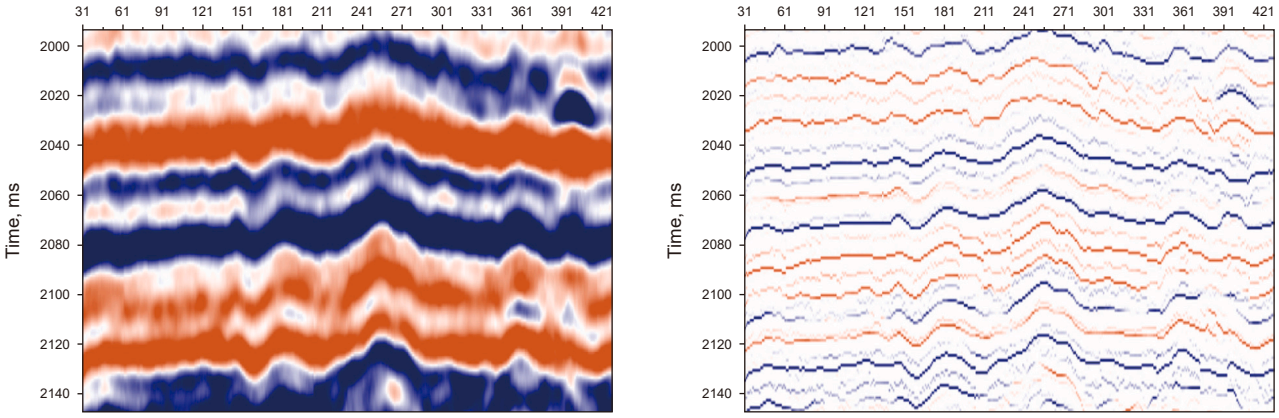

Fig. 11. Comparison of raw data and reflection coefficients.

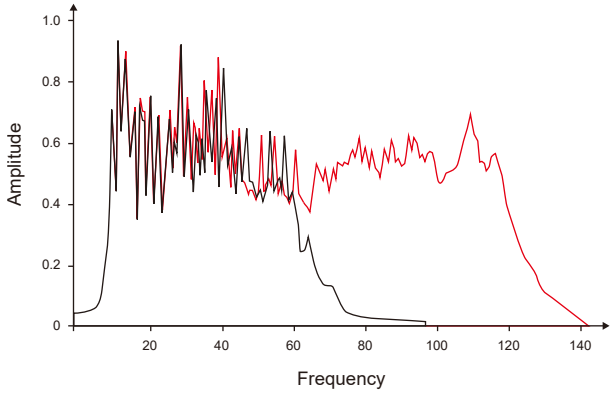

Fig. 12. Spectrum comparison between original and new seismic data.

basin in Ecuador. The main reservoirs are the Cretaceous sandstones of the Hollín Formation and the Napo Formation. The M1 reservoir of the Napo Formation, deposited in a shallow marine shelf environment, contains thin sand bodies in the western part of the basin. Wells drilled in the area (such as M01, M05, M05–1, M05-2, etc.) have an average depth of about 3,300 m, with the M1 reservoir at a depth of approximately 3,000 m. Drilling results indicate that the M1 thin sandstone exhibits rapid lateral variation, with a thickness of about 3–5 m. The dominant frequency of the post-stack seismic data is approximately 42 Hz (Fig. 14), yielding a resolution of about 26 m (one-quarter wavelength), which makes it difficult to identify the seismic reflection characteristics of the sand bodies. Due to the narrow frequency band of the seismic data, traditional sparse spike inversion has low resolution, making it challenging to distinguish reservoirs and predict sand distribution.

The resolution of the processed seismic data is significantly improved (Fig. 15(b)), with clear weak seismic reflections and wave groups corresponding to the original seismic wave groups (Fig. 15(a)). Before processing, the seismic data is about 45 Hz, the effective frequency is 8–55 Hz, and the theoretical maximum cutoff frequency can be identified with a thickness of about 14 m; the seismic profile obtained in this method is about 85 Hz, and the effective frequency is expanded to 7–135 Hz, and the theoretical maximum cutoff frequency can be identified with a thickness of about 5 m. Compared with the original seismic profile, the apparent resolution of the seismic profile obtained by this method is nearly 1 times higher and the effective bandwidth is close to twice the original one. The interpretation horizon of the original seismic data is consistent with the high-resolution data, and this reconstruction method ensures the phase stability of the seismic signal.

On the plane, the RMS seismic attributes of the proposed method (Fig. 16(b)) are clearer than those of the original seismic attributes (Fig. 16(a)), effectively reflecting the outline of the delta and underwater distributary channels, particularly the leaf-shaped channels in the west.

Fig. 17 presents the drilling interpretation for the target area, incorporating results from Gamma ray (GR), spontaneous potential (SP), calcite volume (VOL_CALCITE), quartz volume (VOL_-QUARTZ), and visual geology log (VGL). The GR value of the M1 zone in well M01 is approximately 20API, indicating oil and gas, with an interpreted sandstone thickness of 8.7 ft (Fig. 17(a)). The GR activity value of the M1 layer in wells M05 and M05-1 is about 80API, with no oil or gas shown in the logging, interpreted as mudstone (Fig. 17(b) and (d)). The GR activity in the M1 zone of well M05-2 is about 20API, interpreted as sandstone with a thickness of approximately 15.3 ft (Fig. 17(c)).

In the raw seismic profile, due to low resolution, the seismic reflections of reservoirs and non-reservoirs are located near the zero-crossing point, making it difficult to identify the seismic reflection of the M1 thin sandstone (Fig. 18).

Compared with the raw seismic (Fig. 19), it is obvious that the M01 and M05-2 Wells encountered Compared to the raw seismic data, the processed data clearly show that wells M01 and M05-2 encountered effective sand reflections of the M1 layer, both located in the red weak trough of the newly processed data. The distance between the wells is approximately 3.4 km, indicating good sand continuity. Wells M05 and M05-1 were drilled into the weak peak reflection of mudstone, located 0.4 km and 0.2 km from well M05-2, respectively, showing rapid lateral changes in sandstone. The drilling results from all four wells are consistent with the predictions derived from the newly processed seismic reflections.

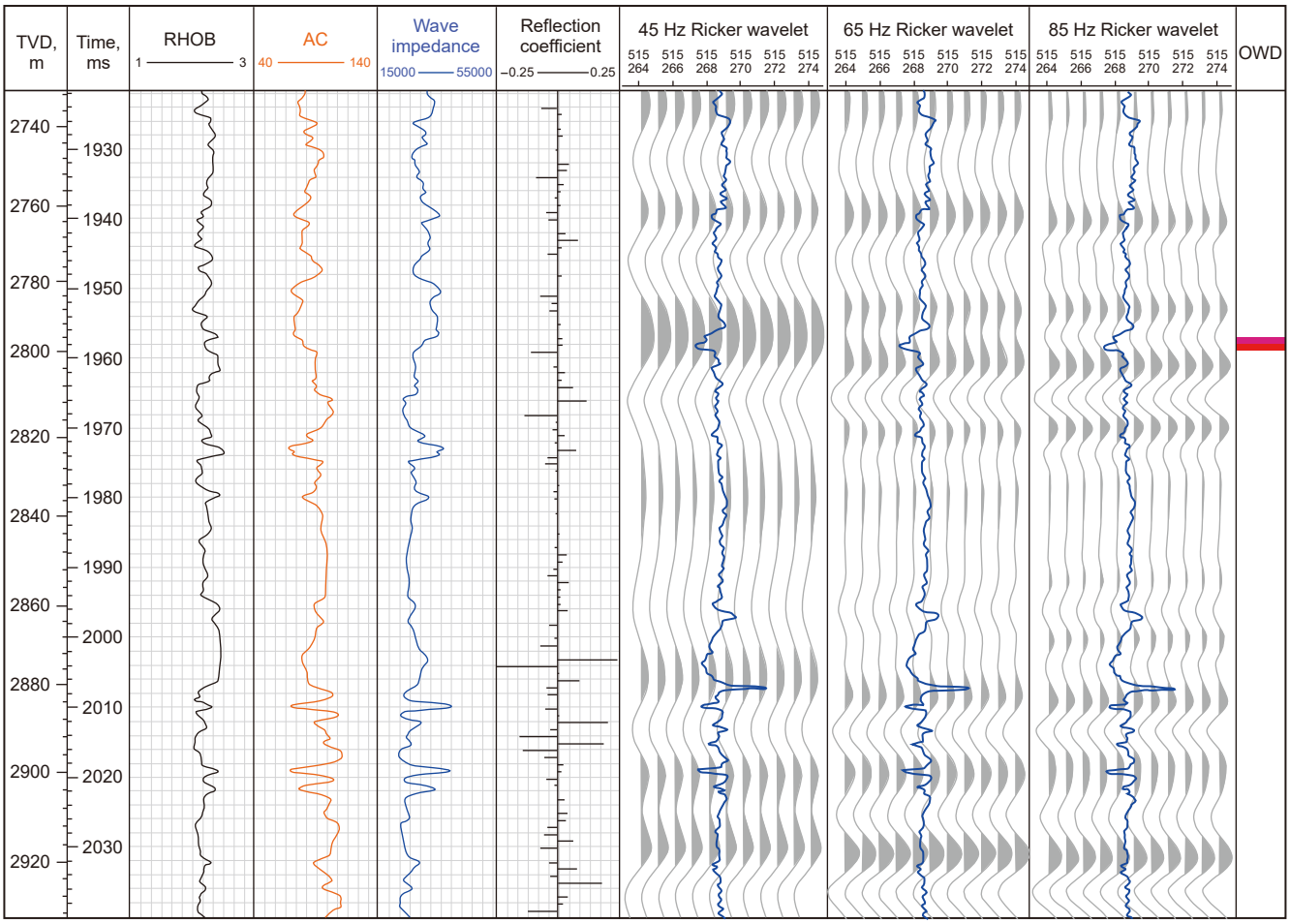

Fig. 13. Synthetic seismic records of Ricker wavelets with different dominant frequencies (TVD: true vertical depth; RHOB: bulk density; AC: acoustic compressional wave slowness; OWD: open hole depth).

6. Discussion

The high-resolution thin sandstone reservoir identification method proposed in this study significantly enhances the accuracy of reservoir geological interpretation through three key technological innovations. 1) Targeted denoising technology effectively preserves the weak reflection signals of thin sandstones, enabling seismic data to clearly delineate the spatial distribution patterns of 2–8 m thin sand bodies, thereby providing a reliable basis for accurately characterizing the macroscopic distribution of reservoirs. 2) Innovative time-varying wavelet modeling technology overcomes the mismatch between traditional fixed wavelets and actual seismic wavelets by constructing a discrete wavelet library. This provides a more accurate time-varying wavelet model for reflection coefficient inversion, significantly improving the recovery accuracy of thin-layer reflection signals. 3) The reflection

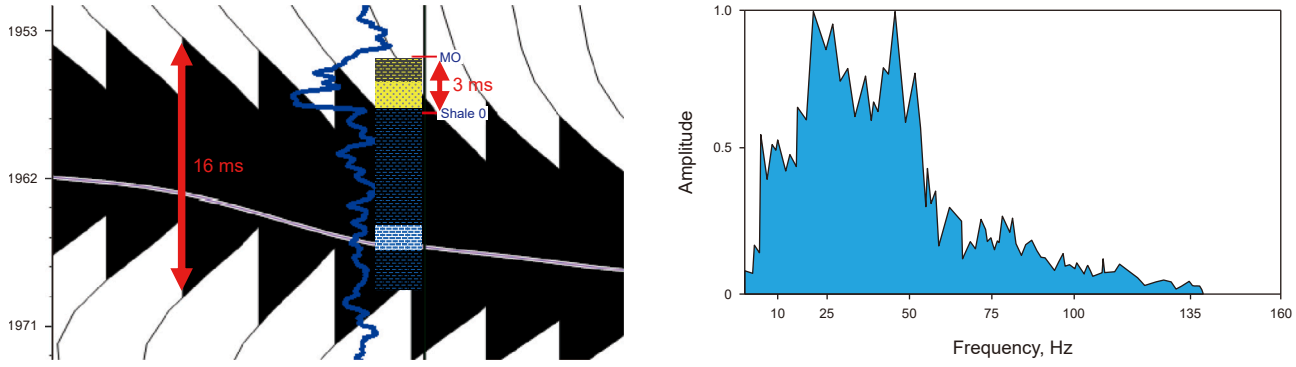

Fig. 14. Original seismic profile and spectrum with well M01.

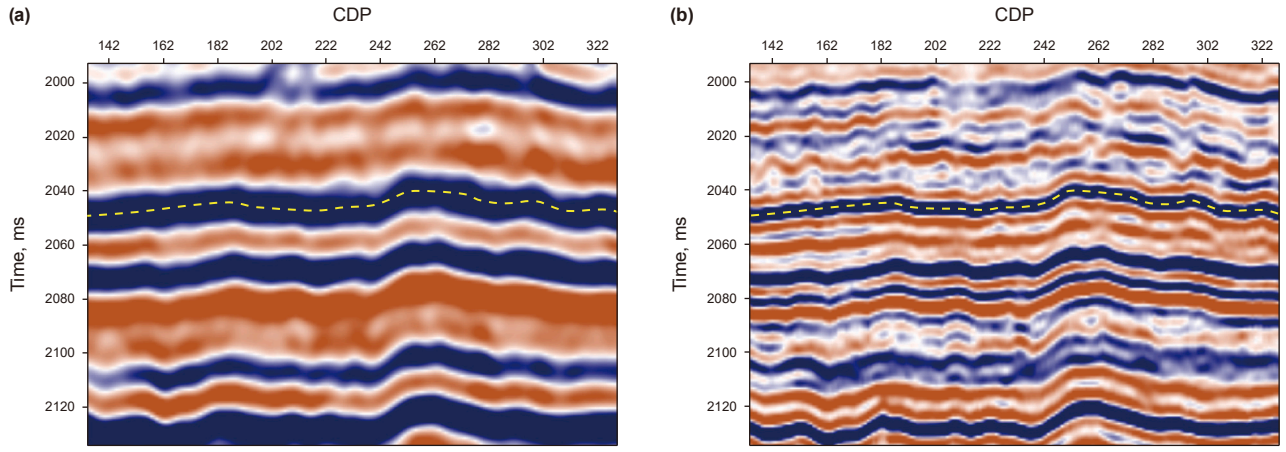

Fig. 15. (**a**) Raw and (**b**) processed seismic profiles.

coefficient inversion technology based on odd-even reflection theory achieves high-precision wave impedance reconstruction, enabling researchers to effectively distinguish between hydrocarbon-bearing reservoirs and dry layers. Its application in the M Oilfield successfully identifies multiple previously overlooked lithologic reservoirs, with drilling results exhibiting high consistency with seismic interpretation.

In the practical application within the 500 km^2 3D work area of the study region, this method leads to significant breakthroughs in geological understanding: it first reveals the continuous distribution characteristics of the M thin sandstone reservoir, correcting the traditional view that the M01 well area is an "isolated reservoir"; it accurately characterizes the spatial configuration relationship of the reservoir in the M05 well area, providing key geological basis for drilling trajectory optimization; and it identifies new hydrocarbon-bearing prospective zones in originally dry well areas, significantly enhancing the exploration success rate in this region. These results confirm the effectiveness of this method in predicting thin sandstone reservoirs and provide reliable technical support for oil and gas exploration under similar geological conditions.

It should be noted that the applicability of this method to complex reservoirs such as carbonate rocks still requires further verification. Compared with thin sandstones, carbonate reservoirs exhibit stronger heterogeneity and more complex pore structures, leading to fundamental differences in their seismic response characteristics. The current method faces the following challenges when dealing with such reservoirs: the targeted denoising workflow may excessively suppress effective signals in fracture-cavity type reservoirs; the time-varying wavelet model struggles to accurately describe the waveform distortion characteristics of pore-fracture-cave composite systems; particularly in reef-flat developed areas, drastic lateral lithological variations significantly increase the uncertainty of inversion results. Therefore, it is necessary to establish more geologically targeted processing workflows, including

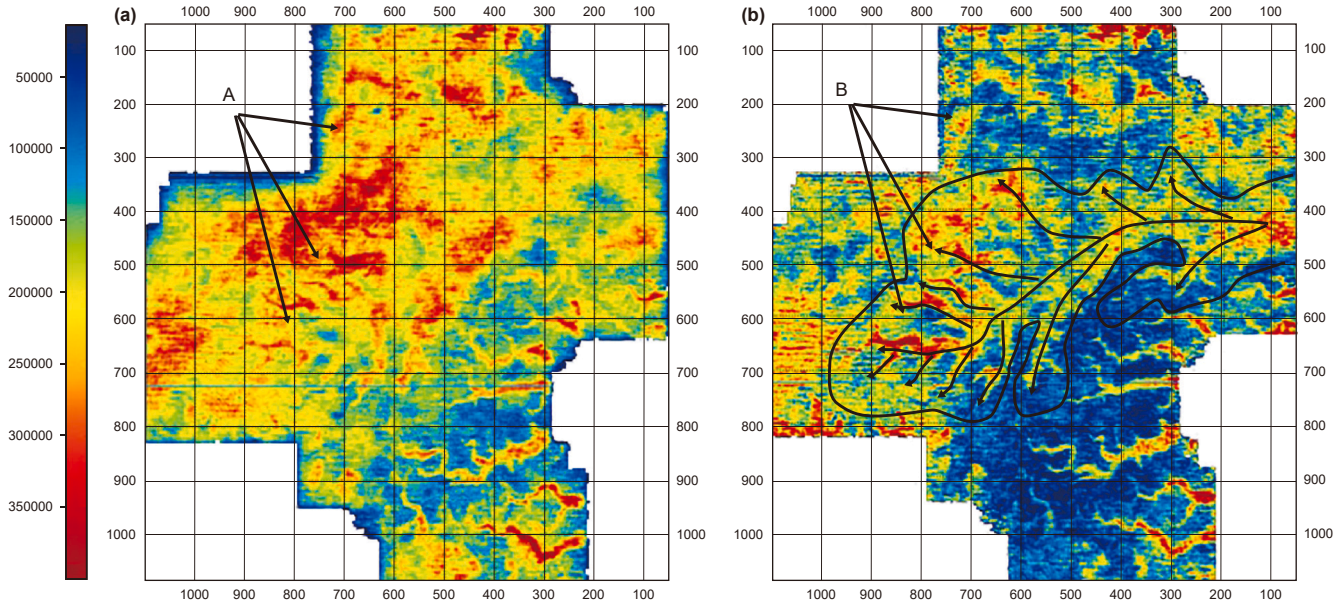

Fig. 16. Raw (**a**) and proposed method result (**b**) seismic RMS amplitude attributes of delta and channel features.

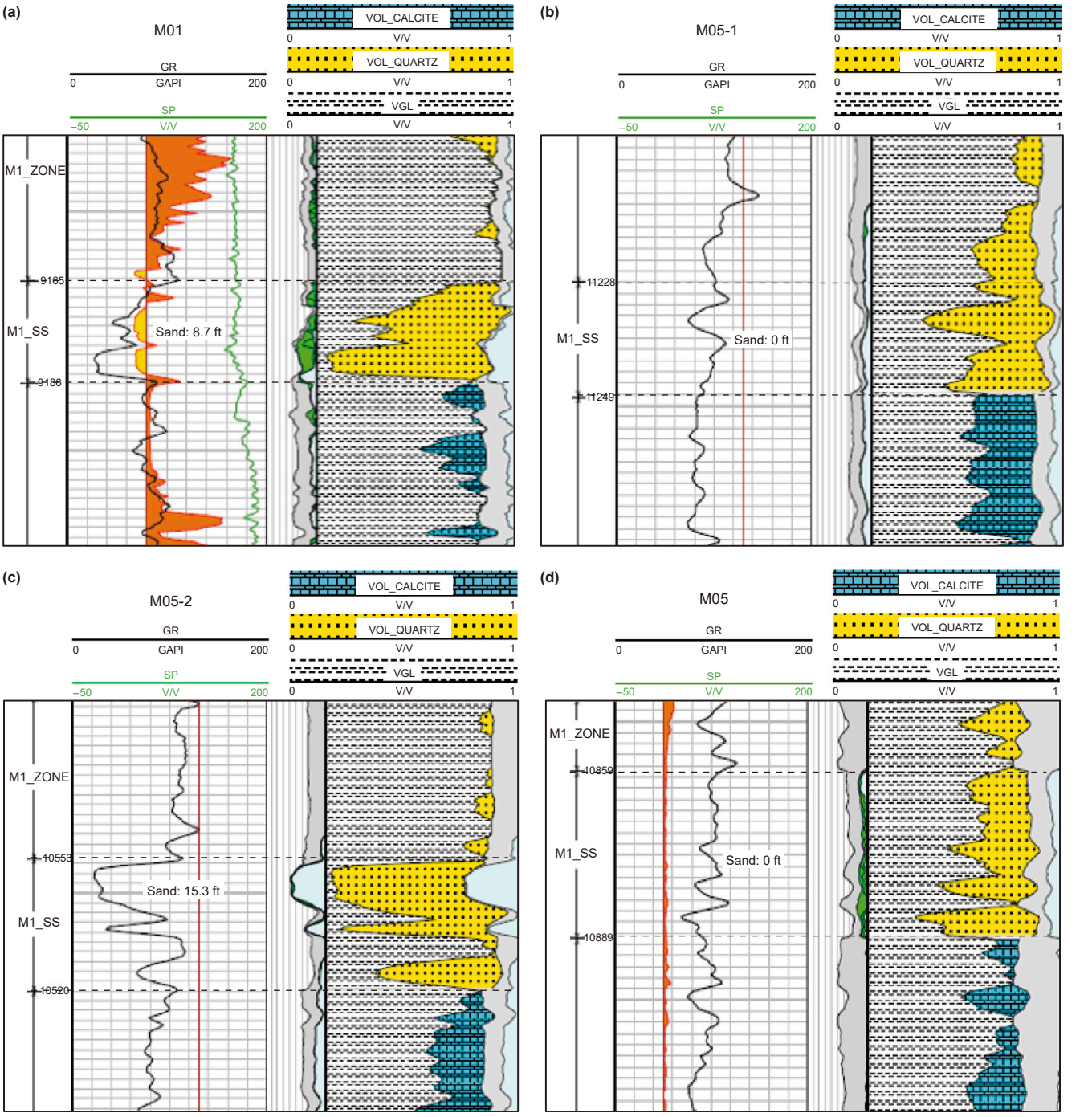

Fig. 17. Well logging interpretation of the drilled target zone.

developing specialized denoising algorithms suitable for fracture-cavity reservoirs and constructing intelligent wavelet models capable of simultaneously characterizing lithofacies and physical property variations.

At the engineering application level, the computational efficiency of the current method still requires further improvement. Subsequent research will focus on optimizing the parallel computing architecture of the inversion algorithm, which is expected to improve computational efficiency by 3–5 times. Concurrently, we will explore rapid inversion strategies based on geological constraints, aiming to reduce the processing cycle to 40% of the current level while maintaining accuracy, thereby better meeting the timeliness requirements of actual production.

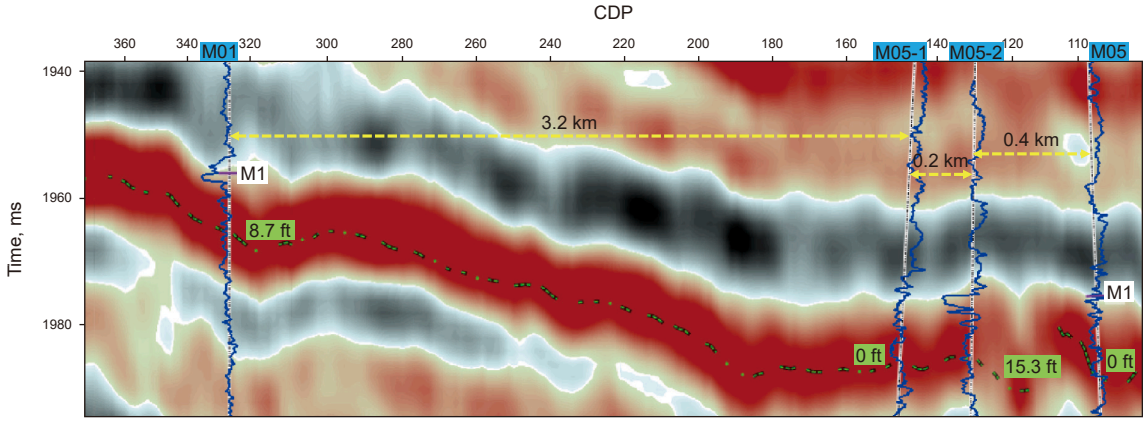

Fig. 18. Raw seismic reflection of drilling points.

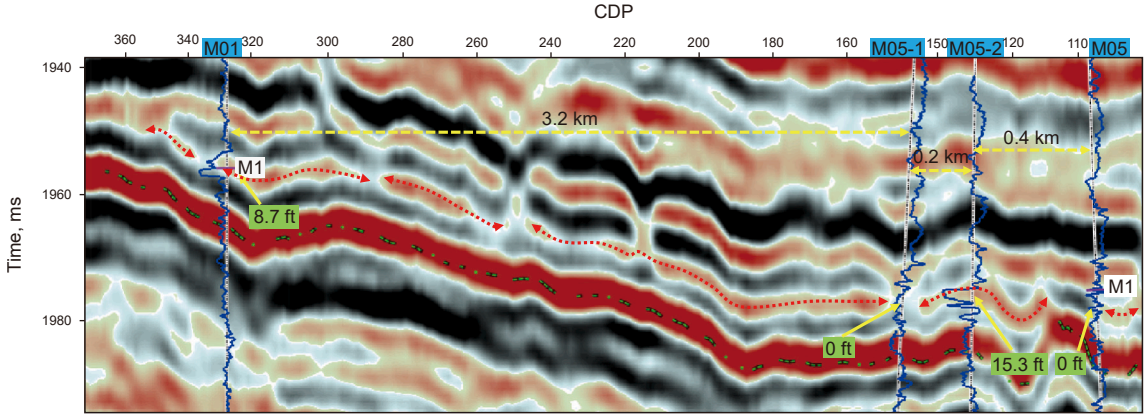

Fig. 19. High-resolution seismic reflection with drilling targets.

7. Conclusion

This study presents a novel approach to thin sandstone identification based on post-stack seismic data, leveraging time-varying wavelet functions and advanced denoising techniques. The method effectively overcomes the limitations of traditional deconvolution, time-varying spectral whitening, inverse *Q* filtering, and spectral inversion, ensuring stable reflection coefficient solutions and improved signal reconstruction. The application in the M oilfield demonstrates its capability to accurately predict 3–5 m ultra-thin reservoirs, with all drilled wells showing perfect consistency with seismic predictions. This technique holds significant promise for the fine description of thin sandstone under similar geological conditions.

CRediT authorship contribution statement

Qi-Ming Zheng: Writing – original draft. **Hui Chen:** Supervision, Funding acquisition. **Qiu-Xiang Zhu:** Writing – review & editing. **Xue-Xiang Gu:** Methodology. **Hai Xu:** Writing – original draft. **Fa-You Li:** Methodology, Formal analysis. **Ben-He Cheng:** Software, Resources. **Yu-Liang Feng:** Supervision, Software. **Chuan Wang:** Visualization, Validation.

Declaration of competing interest

The authors declare that they have no known competing financial interests or personal relationships that could have appeared to influence the work reported in this paper.

Acknowledgements

The authors would like to thank the editors and reviewers for their constructive comments, which will greatly help improve the quality of this article. Also, the authors thank Jie Wu for the contributions to the figures in this article. The authors thank the National Natural Science Foundation of China (Grant Nos. 42574184, 42174164), in part by the Key Program of the Joint Fund of the Science, Technology, and Education of Sichuan Province, China under Grant 2024NSFSC1955; in part by the Natural Science Foundation of Sichuan Province, China under Grants 2024NSFSC0080; in part by the Creative Research Groups of the Natural Science Foundation of Sichuan under Grants 2023NSFSC1984; the Sinopec Petroleum Exploration and Development Research Institute (Grant No. P20072-2) for their financial support.

References

Ameneiro, R., Chiluiza, L., Espinel, G., et al., 2020. Unexpected low-resistivity pay zone while drilling a horizontal well: A case study from the Oriente Basin in Ecuador. In: SPE Latin American and Caribbean Petroleum Engineering Conference, SPE-199092-MS. https://doi.org/10.2118/199092-MS.

Baby, P., Rivadeneira, M., Barragán, R., 2013. Thick-skinned tectonics in the Oriente foreland basin of Ecuador. Geolog. Soci. Spec. Pub. 377 (1), 59–76. https://doi.org/10.1144/SP377.1.

Castagna, J., Sun, S., Siegfried, R., 2003. Instantaneous spectral analysis: Detection of low-frequency shadows associated with hydrocarbons. Lead. Edge 22 (2), 120–127. https://doi.org/10.1190/1.1559038.

Chen, X., He, Z., Huang, D., 2008. Generalized S-transform and its time-frequency filtering. J. Signal Process. 24 (1), 28–31. https://doi.org/10.3969/j.issn.1003-0530.2008.01.007.

Chen, Z., Wang, J., 2015. A spectral inversion method of sparse-spike reflection coefficients based on compressed sensing. Geophys. Prospect. Pet. 54 (4), 459–466. https://doi.org/10.3969/j.issn.1000-1441.2015.04.013.

Chopra, S., Castagna, J., Portniaguine, O., 2006. Seismic resolution and thin-bed reflectivity inversion. CSEG Recorder 31 (1), 19–25. https://library.seg.org/doi/10.1190/1.2369941.

Du, L., Qiu, J., Zhang, Q., et al., 2019. Development and application of a high-fidelity and high-resolution telemetry seismic data acquisition system. Chin. J. Geophys.–Chin. Ed. 62 (10), 3964–3973. https://doi.org/10.6038/cjg2019M0483 (in Chinese).

Fu, Z., Gao, J., Kong, F., et al., 2019. Differential tectonic evolution and a dynamic oil pool in the south of block 17, Oriente Basin. Petrol. Geol. Exp. 41 (2), 222–227. https://doi.org/10.11781/sysydz201902222.

Gabor, D., 1946. Theory of communication. J. Inst. Eng. Electron. 93, 429–457. https://digitallibrary.theiet.org/doi/abs/10.1049/ji-3-2.1946.0074.

Gao, J., Chen, W., Li, Y., et al., 2003. Generalized S transform and seismic response analysis of thin inter-beds. Chin. J. Geophys. 46 (4), 526–532. https://doi.org/10.3321/j.issn:0001-5733.2003.04.015.

Huang, N., Shen, Z., Long, S., 1998. The empirical mode decomposition and the Hilbert spectrum for nonlinear and non-stationary time series analysis. Proceed. Roy. Soci. London. Series A: Math. Phys. Eng. Sci. 454, 903–995. https://doi.org/10.1098/rspa.1998.0193, 1998.

Jiang, L., Chen, Y., Xiao, Y., et al., 2018. A comparison of near-surface Q compensation and surface-consistent deconvolution in the near-surface transition zone. Geophys. Prospect. Pet. 57 (6), 870–877. https://doi.org/10.3969/j.issn.1000-1441.2018.06.009.

Li, F., Ban, S., Wang, G., et al., 2024. Reconstruction of the sedimentary system of the Main-M1 sub-member of the Napo Formation in the Cretaceous series of the oriente Basin, South America and its significance for oil and gas exploration. J. Palaeogeogr. 26 (1), 17–27. https://doi.org/10.7605/gdlxb.2024.01.011.

Li, Y., Song, W., Tang, C., et al., 2021. Complex domain-matching pursuit for near-surface Q-estimate and deep learning modeling. Geophys. Prospect. Pet. 60 (1), 123–135. https://doi.org/10.3969/j.issn.1000-1441.2021.01.012.

Ma, J., Wang, J., Liu, G., 2016. Seismic data noise attenuation and interpolation using singular value decomposition in frequency domain. Geophys. Prospect. Pet. 55 (2), 205–213. https://doi.org/10.3969/j.issn.1000-1441.2016.02.006.

Morlet, J., Arens, G., Fourgeau, E., et al., 1982. Wave propagation and sampling theory—Part II: Sampling theory and complex waves. Geophysics 47 (2), 222–236. https://doi.org/10.1190/1.1441329.

OuYang, M., Wang, D., Li, Z., et al., 2019. Research on CEEMD and wavelet threshold jointed denoising based on compressed sensing. Prog. Geophys. 34 (2), 615–621. https://doi.org/10.6038/pg2019CC0354 (in Chinese).

Pinnegnr, C., Mansinha, L., 2003. The S-transform with windows of arbitrary and varying shape. Geophysics 68 (1), 381–385. https://library.seg.org/doi/10.1190/1.1543223.

Puryear, C., Castagna, J., 2008. Layer-thickness determination and stratigraphic interpretation using spectral inversion: Theory and application. Geophysics 73 (2), R37–R48. https://doi.org/10.1190/1.2838274.

Smith, M., Perry, G., Stein, J., et al., 2008. Extending seismic bandwidth using the continuous wavelet transform. First Break 26 (6), 97–102. https://doi.org/10.3997/1365-2397.26.1288.28410.

Stockwell, R., Mansinha, L., Lowe, R., 1996. Localization of the complex spectrum: The S transform. IEEE Trans. Signal Process. 44 (4), 998–1001. http://ieeexplore.ieee.org/document/492555.

Tong, X., Wang, W., Wang, Y., 2023. PCA matrix denoising is uniform. https://doi.org/10.48550/arXiv.2306.12690.

Wang, E., Nealon, J., 2019. Applying machine learning to 3D seismic image denoising and enhancement. Interpretation 7 (3), SE131–SE139. https://library.seg.org/doi/10.1190/INT-2018-0224.1.

Wang, J., Zhou, X., Cao, M., 2003. Improvement and application of homomorphic deconvolution. Oil Geophys. Prospect. 38 (S1), 27–30. https://doi.org/10.3321/j.issn:1000-7210.2003.z1.005.

Wang, Q., Jiang, X., Wen, B., et al., 2015. Research and application of high-resolution technique based on Gabor transform with carriable time window. China Offshore Oil Gas 27 (6), 19–26. https://doi.org/10.11935/j.issn.1673-1506.2015.06.003.

Wang, S., Chen, H., Hu, Y., et al., 2025. Multichannel seismic resolution enhancement via spectral fitting for thin reservoir characterization. Pet. Sci. 22 (7), 2818–2827. https://doi.org/10.1016/j.petsci.2025.04.008.

Widess, M., 1973. How thin is a thin bed. Geophysics 38 (6), 1176–1180. https://doi.org/10.1190/1.1440403.

Yilmaz, O., 1987. Seismic Data Analysis: Processing, Inversion, and Interpretation of Seismic Data. Society of Exploration Geophysicists, Tulsa, pp. 85–94.

Yun, M., Zhao, Q., Li, X., 2022. Thoughts on seismic resolution and countermeasures for high-resolution exploration. Oil Geophys. Prospect. 57 (5), 1250–1262. https://doi.org/10.13810/j.cnki.issn.1000-7210.2022.05.026.

Zhang, J., Chen, X., Jiang, W., 2021. Review on depth-domain seismic wavelet estimation. Geophys. Prospect. Pet. 60 (3), 353–365. https://doi.org/10.3969/j.issn.1000-1441.2021.03.001.

Zhao, Y., Mao, N., Chen, X., 2021. Self-adaptive gain-limit inverse Q filtering method based on SNR in time-frequency domain. Litholog. Res. 33 (4), 85–92. https://doi.org/10.12108/yxyqc.20210409.

Zhu, S., Sun, P., Zhang, K., et al., 2024. Paleogeographic reconstruction and sedimentary evolution of tidal-dominated estuarine depositional systems: insights from the campanian M1 sandstone formation, Oriente Basin, Ecuador. Mar. Petrol. Geol. 170, 107125. https://doi.org/10.1016/j.marpetgeo.2024.107125.

Zhu, X., Guo, T., Cao, W., et al., 2022. A seismic resolution improvement method based on reflection coefficient inversion. Geophys. Prospect. Pet. 61 (6), 985–993. https://doi.org/10.3969/j.issn.1000-1441.2022.06.004.